Research Article

Enhanced visible-light photocatalytic performance of cadmium sulfide film via annealing treatment

Jun Wang[1] · Cong Liu[1] · Yuquan Wang[1] · Pengfei Shen[2] · Yannan Mu[3] · Fuchao Jia[1] · Tong Zhou[1] · Fei Xing[1] · Guangchao Yin[1] · Meiling Sun[1]

Received: 8 October 2020 / Accepted: 6 November 2020 / Published online: 18 November 2020

Abstract
In this study, cadmium sulfide (CdS) film prepared through a simple homogeneous precipitation method is used for methylene blue degradation. An enhanced visible-light photocatalytic performance of CdS film can be observed after the N_2 annealing treatment. This enhancement in photocatalytic activity can be attributed to the higher crystallinity, better optical absorption, and efficient photogenerated carrier transfer performance of samples. The N_2 annealed CdS films also display the optimum reproducibility in recycling reactions, which is beneficial for its practical application. This study provides a reference for preparing other catalysts with high photocatalytic activity and stability for degradation of dye under visible light.

Keywords CdS · Homogeneous precipitation · Photocatalytic degradation · Visible-light photocatalysis

1 Introduction

Nowadays, the promising and green photocatalysis technology-based semiconductors have capture tremendous concern because it can solve the problems of energy shortage and environmental pollution [1]. Various semiconductor materials have been widely applied on account of their high-light-harvesting efficiency, fast mobility of charge carriers, and various morphologies to photodegrade the pollutants [2–12]. Nevertheless, there remain some crucial deficiencies of many traditional catalysts, including high recombination rate of photogenerated carriers, limited visible-light response, and insufficient specific surface area [13–15], which limits their development and wide application. Therefore, development of novel, cost-effective, and highly efficient visible-light photocatalyst are important for practical applications.

Compared with reported ultraviolet-light photocatalysts, CdS is regarded as a remarkable photocatalyst and shows an outstanding potential in various photocatalytic process. CdS has unique energy levels and a narrow band gap about 2.4 eV, which can effectively make use of visible light to degrade organic pollutants [16–18]. However, the application of CdS is restricted because there are some drawbacks associated with CdS, namely, high recombination rate of photogenerated charge carriers and severe photocorrosion when irradiated by visible light [19]. As reported, to enhance the photocatalytic efficiency of CdS, several feasible methods have been introduced, such as, doping or semiconductor coupling to tune the band gap width and suppress photocorrosion of CdS [20–23]. Regrettably, to the best of our knowledge, satisfactory photocatalytic efficiency based on CdS has not been achieved until now. As a consequence, it is very much

✉ Jun Wang, junwang1819@163.com; ✉ Meiling Sun, sunml@sdut.edu.cn | [1]School of Physics and Optoelectronic Engineering, Shandong University of Technology, Zibo 255000, China. [2]Academy for Advanced Interdisciplinary Studies, Southern University of Science and Technology, Shenzhen 518055, China. [3]Department of Physics and Chemistry, Heihe University, Heihe 164300, China.

requisite to find a successful strategy to improve the photocatalytic activity of CdS.

As is well known, the photocatalytic activity of nanomaterials is strongly dependent on its size, shape, and morphology [24, 25]. Herein, it is of great importance for the formation of CdS with controllable morphology and structure to achieve excellent photocatalytic activity. CdS films have been deposited by a variety of physical and chemical techniques including close spaced sublimation method, electrodeposition, magnetron sputtering, chemical bath deposition method, successive ionic layer adsorption and reaction, and homogeneous precipitation method [26–35]. Compared with the above methods, homogeneous precipitation method is an efficient technique to control the dimensions and size of CdS nanoparticle. In addition, annealing atmosphere also plays a crucial role in constructing definite physicochemical properties of final products. CdS films with different shapes/sizes or colors can be produced by changing the parameters for heat treatment [35–37]. However, it is worth noting that the comparative study of thermal annealing effects under various atmospheres on CdS films prepared by homogeneous precipitation method is very limited. Thus, it is highly desirable to explore the relationship between annealing atmosphere and catalytic performance of CdS films.

Herein, in this study, CdS films annealed under various atmospheres are successfully fabricated and then used for the degradation of MB. The effects of annealing atmosphere on the structure, morphology, UV–Vis absorption, and photoelectrochemical properties of CdS films are thoroughly characterized by various analysis techniques. The results show that annealing atmosphere plays a role in the structure, morphology, UV–Vis absorption, and photoelectrochemical properties of CdS films, which greatly influences the photocatalytic activity of CdS films. Under the irradiation of visible light, the obtained N_2 annealed CdS films exhibit excellent catalytic activity and stability in photocatalytic degradation. This work may provide a new strategy for the design of highly photoactive CdS nanomaterials under visible-light irradiation.

2 Experimental section

2.1 Materials preparation

CdS films are prepared on FTO using a homogeneous precipitation method [38]. Cadmium chloride, urea, thiourea, and deionized water are used for the preparation of CdS films. The deposition temperature is set at 90 °C for 40 min. After completion of the reaction, the as-deposited films are rinsed thoroughly with deionized water for several times to remove the loosely adhered CdS particles. During annealing process, vacuum, N_2, and air atmosphere with different oxygen content and activity in chemistry are conducted. It is identified that N_2 is a relatively inert gas in comparison with vacuum and air, which can be used to reduce the oxygen content during annealing process. In contrast, the air has a high oxygen content. The vacuum is an active gas with strong reducibility, which may react with the as-prepared CdS films. Therefore, the samples are annealed in vacuum, N_2, and air atmosphere at 400 °C for 20 min, respectively.

2.2 Characterization

The morphologies and element distributions of synthesized samples are measured by the field emission scanning electron microscope (FESEM, JEOL JSM-6700F) and energy-dispersive X-ray spectroscopy (EDX). The crystal structure of samples is characterized by X-ray diffraction (XRD, D/max-2500/PC) with Cu Kα radiation ($\lambda = 1.5418$ Å). The photoluminescence (PL) spectra of samples are conducted on a Perkinelmer LS55 fluorescence spectrometer. The UV–Vis absorption spectra are recorded on a UV-3150 double-beam spectrophotometer in the region of 350–600 nm. The Brunauer–Emmett–Teller (BET) measurement is performed via nitrogen (N_2) adsorption–desorption apparatus (BELSORP-max). Photoelectrochemical activity of samples is carried out on an electrochemical workstation (CHI660E) using a standard three-electrode system. CdS films, Pt wire, and Ag|AgCl|KCl(sat) are used as working, counter and reference electrode, respectively. The electrolyte contains a mixture of 0.25 M Na_2S and 0.35 M Na_2SO_3 aqueous solution. The photocurrent density–voltage (*J*–*V*) characteristics and transient photocurrent responses of samples are measured under AM 1.5 illumination provided by a CEL-S500 simulator at 100 mW cm^{-2}. The electrochemical impedance spectroscopy (EIS) measurements are performed at the open circuit potential (− 0.8 V). The photocatalytic performance of CdS films is evaluated by the degradation of MB under visible-light irradiation. In a typical operation, the samples are firstly placed into 200 mL MB aqueous solution (5 mg/L), and remain still in darkness for 15 min, and are then exposed to light from a 500 W Xe lamp equipped with a 420 nm cut-off filter. During the irradiation, 5 mL of the reaction solution is collected at particular intervals. The degradation efficiency of MB is determined by the UV–Vis absorption spectroscopy. The total organic carbon (TOC) analysis of the reaction solution is performed with the Multi N/C 3100 analyzer.

3 Results and discussion

The morphology and elemental composition of CdS films are confirmed by FESEM and EDX, as presented in Fig. 1a–c. It can be observed that after 40 min deposition, a dense and pinhole-free CdS film with uniform nanoparticles is formed on the substrate (Fig. 1a). The thickness of CdS film is about 200 nm (Fig. 1b). The as-prepared films consist of cadmium and sulfur with a molar ratio of 1:1.07, indicating that the films prepared by a homogeneous precipitation method possess proper stoichiometry (Fig. 1c). In addition, during the experimental process, we find that the thickness of CdS film has a direct influence on its properties. CdS films with different thickness are prepared by controlling the corresponding reaction time. From Fig. 2, it can be observed that with the increase in CdS film thickness, the crystallinity of the product improves. The film deposited for 20 min has poor crystallinity, which can be attributed to its uneven morphology (shown in Fig. 3). Significantly, although the film prepared for 60 min shows better crystallinity, the film exhibits increased series resistance in comparison with the film prepared for 40 min (shown in Fig. 4), which can be attributed to its larger thickness (shown in Fig. 3). Hence, in this paper, CdS films deposited for 40 min are used for further investigation.

Figure 5 depicts the XRD patterns of CdS films annealed in vacuum, N_2, and air. As shown, besides the diffraction peaks of FTO substrate, all the diffraction peaks can be aligned to hexagonal CdS structure (JCPDF, no. 80-6). This XRD results confirm that the environment of annealing treatment shows no significant effect on the crystal structure of CdS. However, it is noteworthy that after air-annealing treatment, an additional peak corresponding to CdO can be observed (Fig. 5c). The formation of CdO can be attributed to the oxidation of CdS when the film is annealed in air atmosphere. Besides, the XRD peaks of N_2 annealed CdS films become narrower, suggesting an improved crystalline quality. Based on Debye–Scherrer's formula, the average crystallite size (*D*) of vacuum and N_2

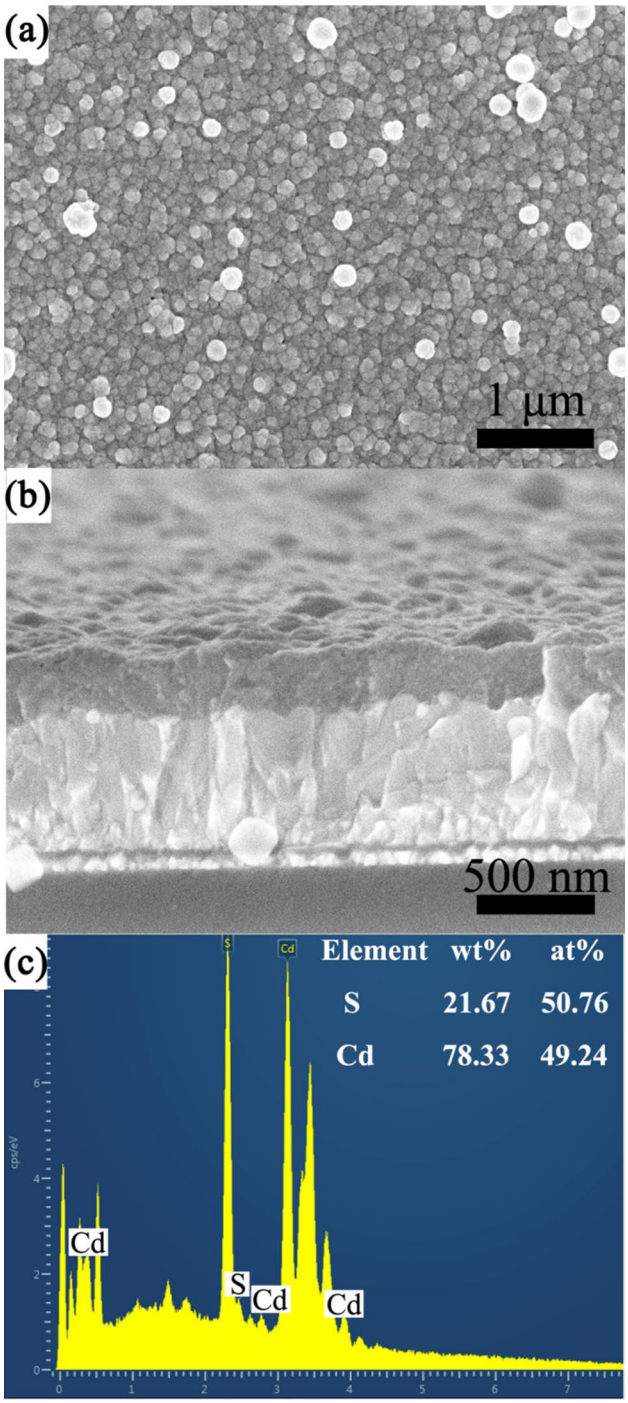

Fig. 1 **a** Top-view and **b** cross-sectional FESEM images of CdS film; **c** EDX spectrum of CdS film

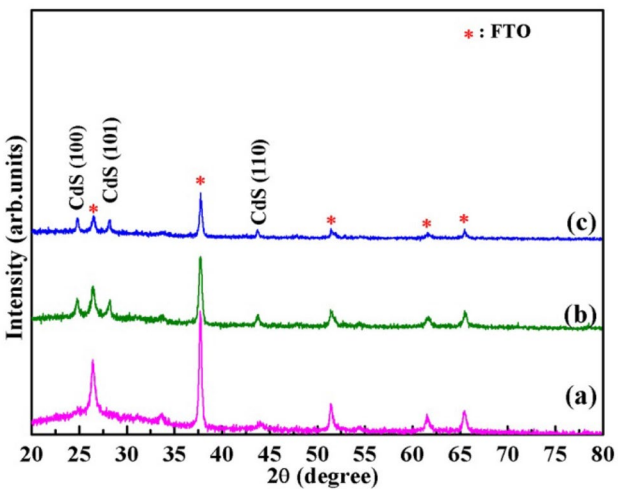

Fig. 2 XRD patterns of CdS thin films prepared at different time: **a** 20 min, **b** 40 min, and **c** 60 min, respectively

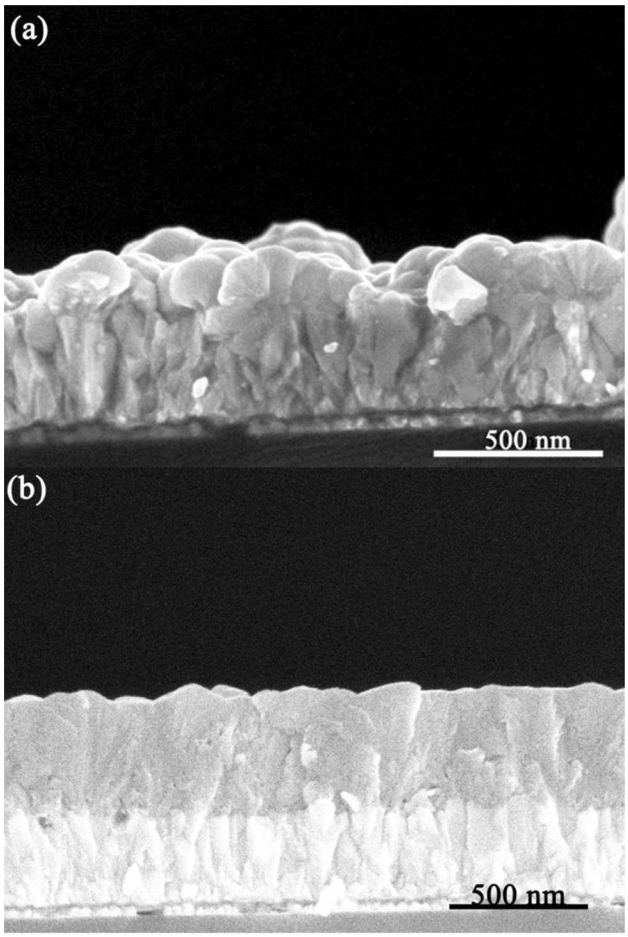

Fig. 3 FESEM images of CdS thin film prepared at **a** 20 min and **b** 60 min, respectively

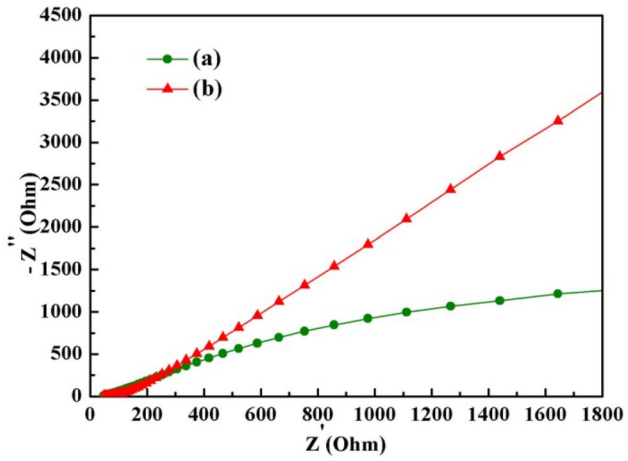

Fig. 4 EIS of CdS thin films prepared at **a** 40 min and **b** 60 min, respectively

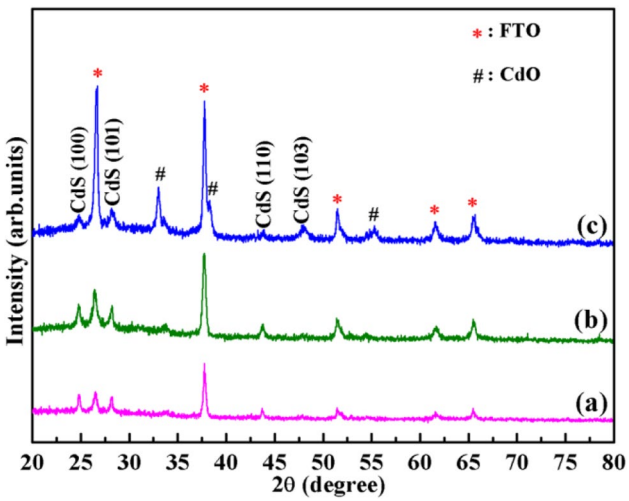

Fig. 5 XRD patterns of CdS thin films annealed in three different atmospheres: **a** vacuum, **b** N_2, and **c** air, respectively

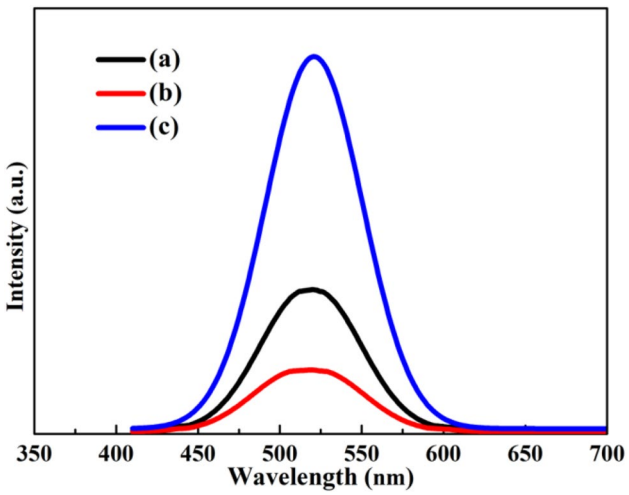

Fig. 6 PL spectra of CdS thin films annealed in three different atmospheres: **a** vacuum, **b** N_2, and **c** air, respectively

annealed CdS film is calculated: $D = \frac{k\lambda}{\beta(hkl)\cos\theta}$. In this formula, shape factor (k) is 0.9, λ is the wavelength of the X-ray source, $\beta(hkl)$ is the "full width at half maximum", and θ is the diffracting angle. The average crystallite sizes for vacuum and N_2 annealed CdS films are found to be approximately 80 nm and 180 nm, respectively. Thus, it can be concluded that the enhanced crystallinity of N_2 annealed CdS films can be attributed to its improved crystallite size. Additionally, to further examine the effect of annealing atmospheres on the crystallinity of samples in details, PL spectra of CdS films are employed at room temperature. Generally speaking, the film with better

crystallinity suggests less recombination of photogenerated carriers, thus leading to a lower PL intensity. As depicted in Fig. 6, PL intensity of the N_2 annealed CdS films decreases significantly. Therefore, the PL result combining with XRD result indicates CdS film annealed in N_2 has better crystallinity, which can be attributed to be one of the reasons for its superior photocatalytic activity.

FESEM images are obtained to investigate the influence of annealing atmospheres on the morphologies of as-synthesized CdS films (Fig. 7a–c). Obviously, annealing atmospheres significantly affect the surface morphologies of films. As shown in Fig. 7a, a large number of small packed particles can be observed on the surface of the film annealed in vacuum, and these particles are connected tightly and have a clear boundary between each. When the film is annealed in N_2, apparently, many small packed particles disappear, and the surface of CdS film becomes much smoother and more uniform (Fig. 7b). This different phenomenon may be explained as follows. In fact, the reorganization of the film occurs at all annealing process. The recrystallization process may densify the film and some of the small grains coalesce together to form a continuous film with few grain boundaries [39, 40]. Nevertheless, when the film is annealed in vacuum atmosphere, besides reorganization of the film, some of the sulfur will evaporate from the film [41, 42]. This effect leaves larger unfilled inter-granular volume on the surface of CdS film. Therefore, an entirely different microstructure and morphology of CdS film can be created. Similar change in surface features can also occur when the film is annealed in air (Fig. 7c). The grain size of CdS nanoparticles increases, but the interval between the particles becomes much wider, and some pinholes can be observed. More importantly, as shown from the low magnification image (the inset in Fig. 7c), the heat treatment under air atmosphere results in some cubes on the surface of CdS films. EDX data are obtained to further confirm the composition of these cubes, as illustrated in Fig. 7d. Notably, the EDX spectrum describes the presence of cadmium and oxygen, indicating that the composition of this structure is CdO. This result is also consistent with the aforementioned analysis based on the XRD measurement (Fig. 5). The formation of CdO can be attributed to its lower requirement for activation energy in comparison with that of sulfur oxides formation during annealing process. Hence, when CdS film is annealed in air, the formation of CdO on the surface of films can be observed. Similar phenomenon has also been observed by other researchers [43, 44]. In addition, to verify the likely uptake and influence of residual gas or ambient gas on the studied samples, the cross-sectional elemental mapping images of CdS film annealed in N_2 is also exhibited in the inset of Fig. 7b. It is clear that the elements of cadmium and sulfur are well distributed, and no other elements such as C, N, H, and O appear, suggesting the high purity of the film. Indeed, during heat treatment process, a range of different reactions such as oxygen absorption or desorption, creation and annihilation of vacancy–interstitial pairs of cadmium ions, and sulfur evaporation will occur on the surface of CdS film at various atmospheres. As for CdS film, the structure and morphology changes may be ascribed to the different evaporation of sulfur atoms from the CdS films under different annealing atmospheres [45]. A uniform dense CdS film with better structural quality can be obtained when annealed in N_2.

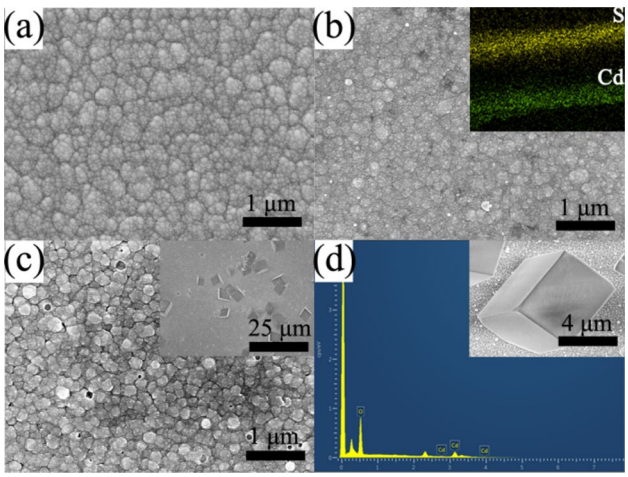

Fig. 7 FESEM images of CdS thin films annealed in three different atmospheres: **a** vacuum, **b** N_2, and **c** air, respectively; **d** EDX spectrum of CdO

The N_2 adsorption–desorption, BET surface area and pore size distribution are conducted to verify the specific surface area and pore structures of as-synthesized samples. Figure 8 shows the absorption–desorption isotherms of CdS films annealed in vacuum, N_2, and air, respectively. As shown in Fig. 8, typical type-IV characteristics of the isotherms of various samples can be observed, suggesting the mesoporous existence. This can facilitate the adsorption of organic pollutants. The BET specific surface areas are calculated to be 20.409 $m^2\ g^{-1}$, 21.749 $m^2\ g^{-1}$ and 25.899 $m^2\ g^{-1}$ for vacuum, N_2 and air annealed CdS film, respectively. Among the series of samples, the air annealed CdS film exhibits the largest specific surface area, which can be attributed to the large cubes on the surface of films. This result also reveals that the excellent photocatalytic performance of N_2 annealed CdS film can be due to its efficient electron transfer process. The pore size distribution of samples is calculated by using the Barrett–Joyner–Halenda (BJH) method according to the desorption branch. The estimated pore size of vacuum, N_2, and air annealed CdS films is approximately

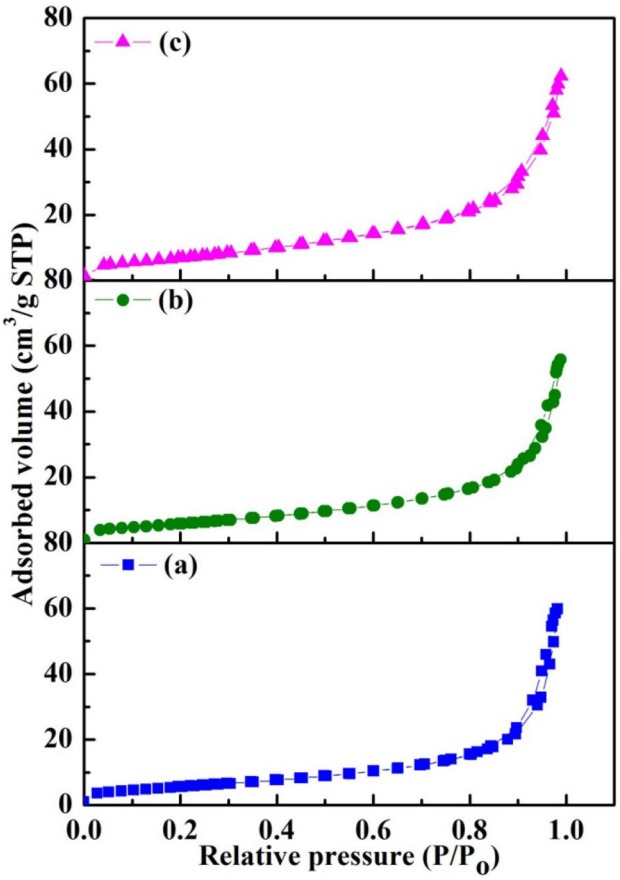

Fig. 8 Nitrogen adsorption–desorption isotherm of CdS films annealed in three different atmospheres: **a** vacuum, **b** N_2, and **c** air, respectively

18.12 nm, 14.877 nm, and 15.855 nm, respectively. According to the results, it can be seen that all the samples have mesoporous structure, facilitating the diffusion of the organic pollutants.

The influence of annealing atmosphere on the optical absorption performance of CdS film is examined using the UV–Vis spectrometer. As is shown in Fig. 9, compared to the air annealed CdS film, the absorption edge of CdS films annealed in N_2 and vacuum obviously shifts to longer wavelength, and an obvious increase in absorbance of films can also be observed. These changes can be attributed to their better growth of the nanocrystalline grain and increased particle size after heat treatment. Among all the films, the N_2 annealed CdS films exhibit the highest absorptivity, suggesting that when the sample is irradiated, it can produce many effective photogenerated carriers and further enhance the photocatalytic activity. The air annealed CdS films show a poor absorptivity, which can be related to the formation of CdO [42]. As discussed above, it can be concluded that annealing atmosphere plays a key role in the enhancement of crystallinity and optical absorption ability of CdS films, which makes CdS films potential application future in the degradation of pollutants.

It is widely recognized that charge separation is a very important process for photodegradation of pollutants. Many photogenerated carriers should be transfer to the surface of sample, and then create a large number of free radicals. These generated radicals are good oxidizers to decompose the organic dye [46–48]. Hence, photocatalytic activity is strongly dependent on the separation and transfer efficiency of photogenerated carriers in the catalysts [49]. In this work, the *J–V* characteristics, photo-current tests, and EIS measurements are measured to get more insight into the interface charge transfer [50, 51]. Shown in Fig. 10 are *J–V* curves of CdS films. It can be observed

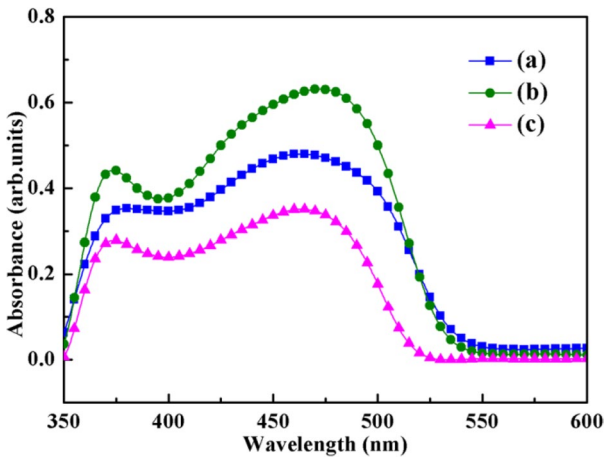

Fig. 9 UV–Vis absorption spectra of CdS films annealed in three different atmospheres: **a** vacuum, **b** N_2, and **c** air, respectively

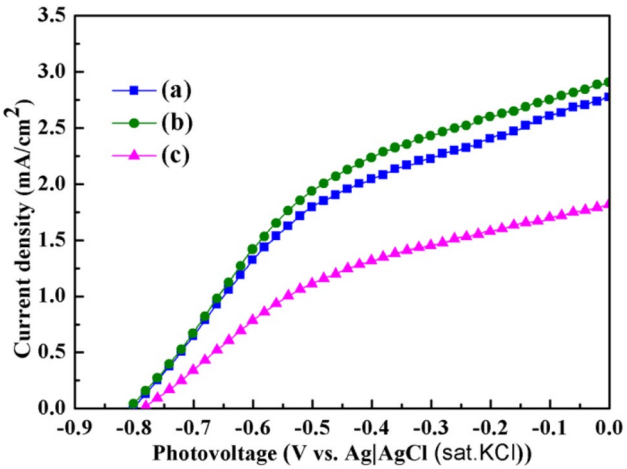

Fig. 10 The *J–V* characteristics of CdS films annealed in three different atmospheres: **a** vacuum, **b** N_2, and **c** air, respectively

that the open circuit photopotential of all the samples is approximately the same, and the current density has remarkable differences. In particular, CdS films annealed in N_2 exhibit the highest photocurrent with the value of 2.91 mA cm^{-2}. The superior performance arises from its enhanced optical absorption, which can generate more photogenerated carriers between the interface of CdS films and the polysulfide electrolyte. In contrast, one significant decrease in photocurrent should be noted when the films are annealed in air, illustrating lower carrier-separation efficiency. This behavior can be attributed to the grain boundaries formed by CdO cubes. Figure 11a presents the photocurrent transient response for all the samples, which are obtained by several on–off treatment cycles of intermittent visible-light illumination. Obviously, under the visible-light irradiation, CdS films annealed in N_2 reveal the best photocurrent response, suggesting that the films have superior separation efficiency of photogenerated carriers. In contrast, the transient photocurrent response of CdS films annealed in air is poor, indicating the appearance of some recombination centers of photogenerated carriers in films. These phenomenon can be explained by EIS measurement. As is shown in Fig. 11b, CdS films annealed in N_2 show the smallest arc radius of the semicircle than the other two samples, suggesting the enhanced separation and transfer efficiency of photogenerated charge. For air annealed CdS films, the sample has a relatively large diameter over the semicircular Nyquist plot, that is, the resistance is higher during charge transfer process as compared to N_2 annealed CdS films. Consequently, annealing atmosphere has a great influence on the separation and transfer of photogenerated carriers and finally may influence the photocatalytic performance of samples.

To understand the effect of annealing atmosphere on the visible-light photocatalytic degradation activity of the as-prepared CdS films, the photocatalytic experiments are conducted. Figure 12a–c presents the changes in the absorption spectra of MB versus irradiation time with the presence of CdS films under visible-light irradiation. The typical progressive decrease in the peak intensity of MB at 664 nm (characteristic absorption peak for MB) is observed, which indicates the photodegradation of MB under visible-light illumination. Upon comparing the photocatalytic removal of MB, CdS films annealed in N_2 have excellent photocatalytic degradation efficiency to MB than other samples, and the absorption at wavelength of 664 nm almost completely disappears after 60 min of irradiation. Moreover, no new absorption bands can be observed during the process of photodegradation, which confirm the complete photodegradation of the MB aqueous solution. In this work, C/C_0 is calculated to evaluate the degradation rate. As presented in Fig. 12d, during the dark period, all the materials show strong adsorption because of their mesoporous structure, and the obtained N_2 annealed CdS films show the highest adsorption ability, which is is beneficial for photodegradation of MB. When all the films are illuminated with visible light, for comparison, CdS films annealed in N_2 show the highest photocatalytic degradation efficiency than others, and in the first 15 min, a sharp decrease in the concentration of MB can be indicated by the decrease in the intensity of absorption peaks (Fig. 12b). The removal rate of MB reaches maximum value of 99.98% after 60 min. The *k* values of MB degradation are also estimated. The values are 0.026/min, 0.044/min, and 0.012/min for the vacuum, N_2 and air annealed CdS films, respectively. It can be seen that the N_2 annealed CdS films exhibit the highest degradation rate constant. More importantly, the mineralization ability of the as-prepared

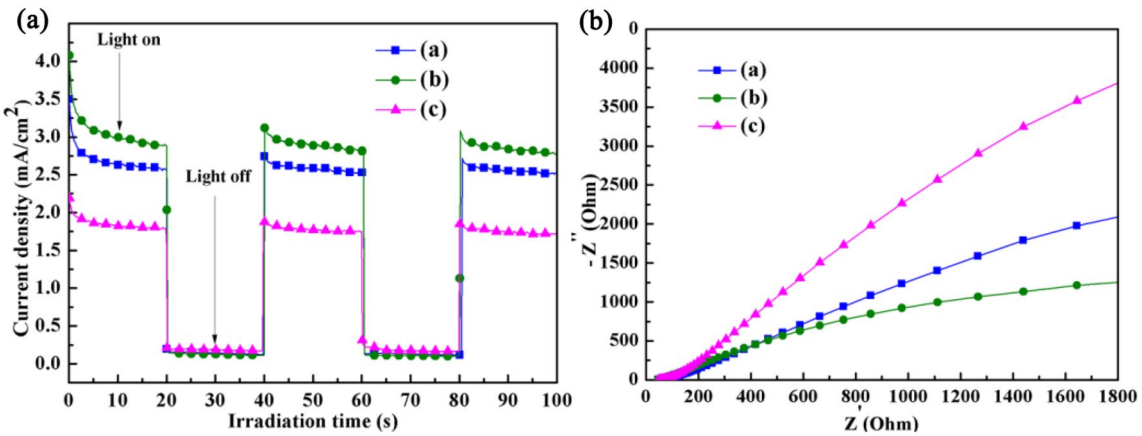

Fig. 11 **a** Transient photocurrent responses and **b** EIS of CdS films annealed in three different atmospheres: (a) vacuum, (b) N_2, and (c) air, respectively

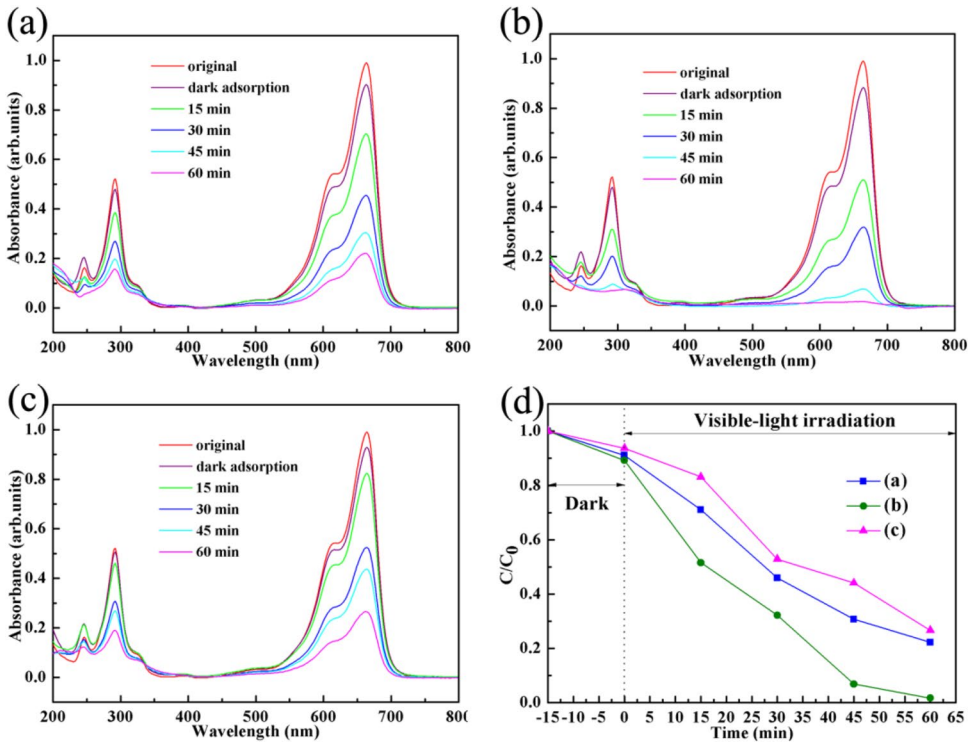

Fig. 12 Absorption changes to an aqueous solution of MB in the presence of CdS films annealed in three different atmospheres: **a** vacuum, **b** N_2, and **c** air, respectively; **d** comparison of the photocatalytic activity of CdS films for the photocatalytic decomposition of MB under visible-light irradiation

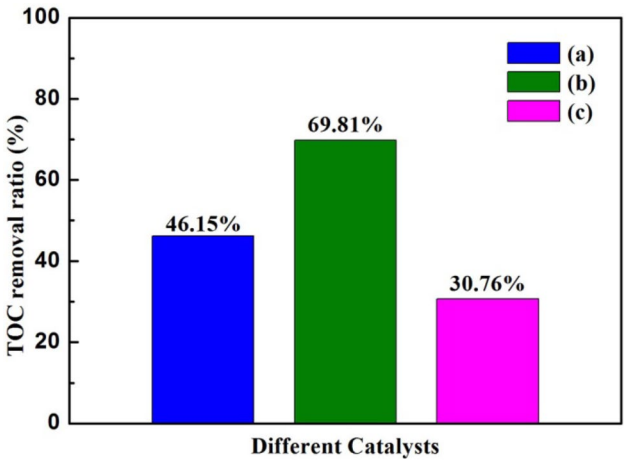

Fig. 13 TOC removal ratio of CdS films annealed in three different atmospheres: **a** vacuum, **b** N_2, and **c** air, respectively

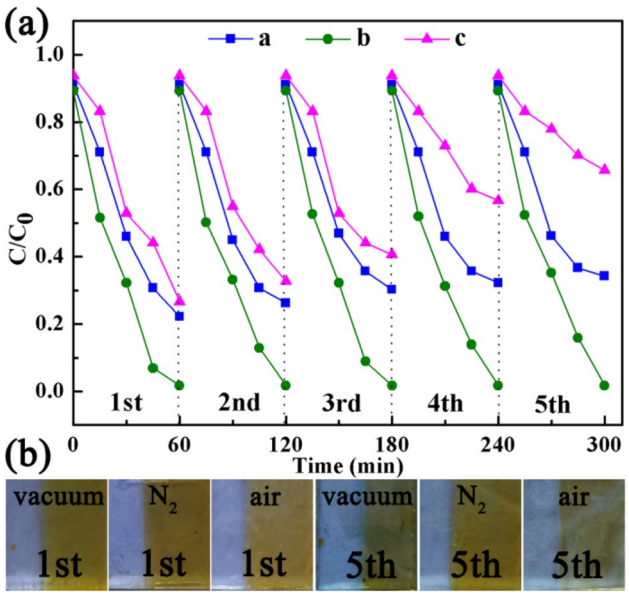

Fig. 14 **a** Cycling runs for photocatalytic degradation of MB over CdS films annealed in: a: vacuum, b: N_2, and c: air, respectively. **b** Figures of as-synthesized CdS films after the first time and fifth degradation cycles

CdS films is also studied. As is clearly depicted in Fig. 13, compared to other samples, the N_2 annealed CdS films display excellent TOC mineralization capacity and the mineralization efficiency reaches about 69.81% within 60 min of reaction, indicating a promising application potential for removal of organics from contaminated water. This observation is also in accordance with the photocatalytic degradation results as shown in Fig. 12. The above results demonstrate that annealing conditions have a great influence on the photocatalytic activity of CdS films. The N_2 annealed CdS films exhibit high photocatalytic activity, which could be attributed to the efficient visible-light utilization and high-efficiency charge separation and transfer in films. Therefore, appropriate annealing conditions can

significantly improve the photoactivity of CdS, which can also be expected to be used for preparing other catalysts.

Besides activity, stability is also a vital parameter for practical application of photocatalysts. The stability of as-prepared CdS films is investigated by five repeated MB degradation experiments, as depicted in Fig. 14a. As compared with the first time degradation ratio, the photocatalytic activity of the CdS films annealed in N_2 still maintains a high level even after using for five cycles. This result describes favorable recycling activity of CdS film annealed in N_2. For CdS films annealed in vacuum, the photocatalytic activity of the sample is reduced slightly by recycling photocatalytic reactions, and a significant change in color of the sample can be observed, suggesting that the sample is destroyed during the degradation of MB (Fig. 14b). Similarly, for the air annealed CdS films, the rate of MB degradation decreases significantly and CdS films clearly peel-off from the substrate after five degradation cycles, as shown in Fig. 14b. This phenomenon can be attributed to the photocorrosion of CdS [52] during the reaction. Meanwhile, to confirm the stability of the photocatalyst, XRD patterns of fresh and used N_2 annealed CdS films (after five cycles) are shown in Fig. 15. One can notice that no change in crystal planes can be observed of N_2 annealed CdS films before and after five times repeat tests. This result also indicates excellent stability of N_2 annealed CdS films. Moreover, RhB as an another dye pollutant is used to evaluate the photocatalytic activity of CdS. It can be seen that the obtained N_2 annealed CdS films can also exhibit excellent photocatalytic degradation rate for RhB of approximately 93% in 60 min under visible light irradiation (Fig. 16). This result indicates that the as-prepared CdS films can also have excellent photocatalytic performance

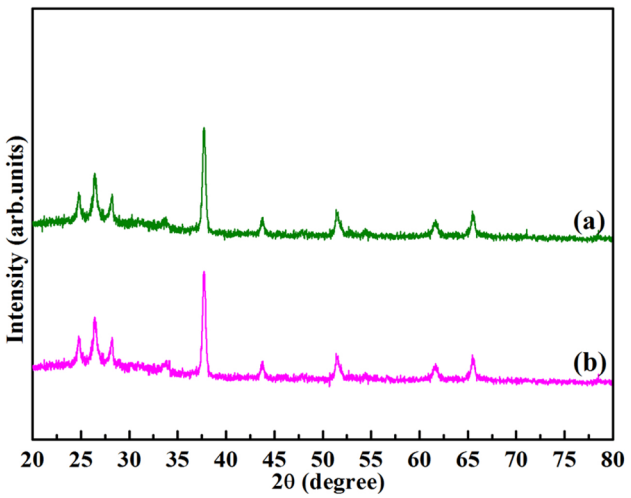

Fig. 15 XRD patterns of **a** fresh and **b** used CdS thin films (after five cycles)

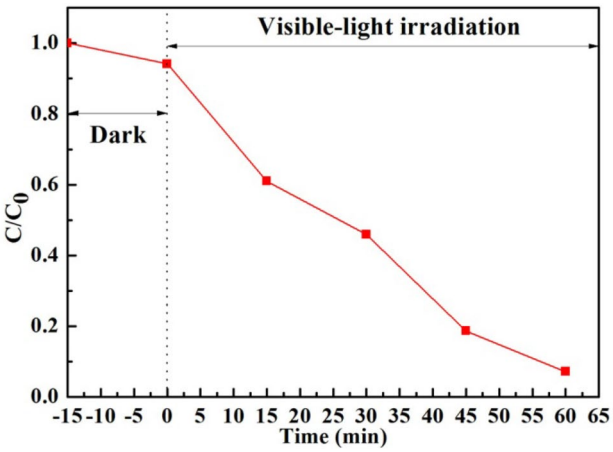

Fig. 16 The photocatalytic activity of CdS films for the photocatalytic decomposition of RhB under visible-light irradiation

for other colorless pollutants. Overall, due to the excellent photocatalytic activity and favorable recycling performance, the CdS films annealed in N_2 is an excellent photocatalyst. More importantly, in comparison with the conventional powder photocatalysts, CdS films grown on FTO substrate are easier to use, and many problems in the photo-catalysis process such as the aggregation and the bleeding of the conventional powder photocatalyst can be avoided.

4 Conclusions

In summary, CdS films annealed under different atmosphere are successfully synthesized and used for efficient MB photodegradation under visible-light irradiation. The morphology, crystallization, UV–Vis absorption, photoelectrochemical and photocatalytic properties of the as-obtained CdS films are characterized. Among all the synthesized samples, the N_2 annealed CdS films exhibit higher crystallinity, remarkable photoabsorption capacity and photoelectrochemical performance, which are all beneficial for the enhancement of photocatalytic capability. In addition, according to the results of recycling photocatalytic experiments, the N_2 annealed CdS films have good repeatability. Therefore, CdS films with high photocatalytic efficiency and stability are potentially applicable in removal of organic pollutants.

Acknowledgements This work was financially supported by Natural Science Foundation of Shandong Province, China (Grant No. ZR2019QF018), National Natural Science Foundation of China (Grant Nos. 61904098, 11904209) and Natural Science Foundation of Heilongjiang Province of China (Grant No. 2017001).

Compliance with ethical standards

Conflict of interest The authors declare that they have no conflict of interests.

References

1. Ling LL, Feng YW, Li H, Chen Y, Wen JY, Zhu J, Bian ZF (2019) Microwave induced surface enhanced pollutant adsorption and photocatalytic degradation on Ag/TiO_2. Appl Surf Sci 483:772–778
2. Kang XL, Song XZ, Han Y, Cao JK, Tan ZQ (2018) Defect-engineered TiO_2 hollow spiny nanocubes for phenol degradation under visible light irradiation. Sci Rep 8:5904
3. Zhao GD, Sun ML, Liu XL, Xuan JY, Kong WC, Zhang RN, Sun YP, Jia FC, Yin GC, Liu B (2019) Fabrication of CdS quantum dots sensitized ZnO nanorods/TiO_2 nanosheets hierarchical heterostructure films for enhanced photoelectrochemical performance. Electrochim Acta 304:334–341
4. Shekofteh-Gohari M, Habibi-Yangjeh A, Abitorabi M, Rouhi A (2018) Magnetically separable nanocomposites based on ZnO and their applications in photocatalytic processes: a review. Crit Rev Environ Sci Technol 48:806–857
5. Pirhashemi M, Habibi-Yangjeh A, Pouran SR (2018) Review on the criteria anticipated for the fabrication of highly efficient ZnO-based visible-light-driven photocatalysts. J Ind Eng Chem 62:1–25
6. Poornaprakash B, Chalapathi U, Poojitha PT, Vattikuti SVP, Park S-H (2019) CdS: Eu quantum dots for spintronics and photocatalytic applications. J Mater Sci: Mater Electron 30:8220–8225
7. Akhundi A, Habibi-Yangjeh A, Abitorabi M, Pouran SR (2019) Review on photocatalytic conversion of carbon dioxide to value-added compounds and renewable fuels by graphitic carbon nitride-based photocatalysts. Catal Rev 61:595–628
8. Vattikuti SVP, Nagajyothi PC, Shim J (2019) Fabrication of CdS quantum dot/Bi_2S_3 nanocomposite photocatalysts for enhanced H_2 production under simulated solar light. J Mater Sci: Mater Electron 30:5681–5690
9. Vattikuti SVP, Ngo I-L, Byon C (2016) Physicochemcial characteristic of CdS-anchored porous WS2 hybrid in the photocatalytic degradation of crystal violet under UV and visible light irradiation. Solid State Sci 61:121–130
10. Akhundi A, Badiei A, Ziarani GM, Habibi-Yangjeh A, Muñoz-Batista MJ, Luque R (2020) Graphitic carbon nitride-based photocatalysts: toward efficient organic transformation for value-added chemicals production. Mol Catal 488:110902
11. Yu H, Huang BB, Wang H, Yuan XZ, Jiang LB, Wu ZB, Zhang J, Zeng GM (2018) Facile construction of novel direct solid-state Z-scheme AgI/BiOBr photocatalysts for highly effective removal of ciprofloxacin under visible light exposure: mineralization efficiency and mechanisms. J Colloid Interface Sci 522:82–94
12. Poornaprakash B, Chalapathi U, Poojitha PT, Vattikuti SVP, Park S-H (2019) Influence of gadolinium (III) doping on the structural, optical, magnetic, and photocatalytic properties of CdS quantum dots. Mater Sci Semicond Proc 100:73–78
13. Ca-Flores U, La-Romero J, Zá-Medina J, Mu-Batista MJ, Hu-Acuña R, Ri-Muñoz EM, Cortés JA (2016) Enhanced photocatalytic activity of MWCNT/TiO_2 heterojunction photocatalysts obtained by microwave assisted synthesis. Catal Today 266:102–109
14. Zalfani M, Hu ZY, Yu WB, Mahdouani M, Bourguiga R, Wu M, Li Y, Tendeloo GV, Djaoued Y, Su BL (2017) $BiVO_4$/3DOM TiO_2 nanocomposites: effect of $BiVO_4$ as highly efficient visible light sensitizer for highly improved visible light photocatalytic activity in the degradation of dye pollutants. Appl Catal B Environ 205:121–132
15. Zhang Q, Chen JX, Xie YY, Wang MZ, Ge XW (2016) Inductive effect of poly(vinyl pyrrolidone) on morphology and photocatalytic performance of Bi_2WO_6. Appl Surf Sci 368:332–340
16. Sun ML, Liu XL, Zhao GD, Kong WC, Xuan JY, Tan SG, Sun YP, Wei SL, Ren JF, Yin GC (2019) Sn^{4+} doping combined with hydrogen treatment for CdS/TiO_2 photoelectrodes: an efficient strategy to improve quantum dots loading and charge transport for high photoelectrochemical performance. J Power Sources 430:80–89
17. Solakidoua M, Giannakas A, Georgiou Y, Boukos N, Louloudi M, Deligiannakis Y (2019) Efficient photocatalytic water-splitting performance by ternary CdS/Pt-N-TiO_2 and CdS/Pt-N, F-TiO_2: interplay between CdS photo corrosion and TiO_2-dopping. Appl Catal B Environ 254:194–205
18. Zhuang HQ, Cai ZP, Xu WT, Zhang XY, Huang ML, Wang XX (2019) Constructing 1D CdS nanorod composites with high photocatalytic hydrogen production by introducing the Ni-based cocatalysts. Catal Commun 120:51–54
19. Huang MN, Yu JH, Deng CS, Huang YH, Fan MG, Li B, Tong ZF, Zhang FY, Dong LH (2016) 3D nanospherical $Cd_xZn_{1-x}S$/reduced graphene oxide composites with superior photocatalytic activity and photocorrosion resistance. Appl Surf Sci 365:227–239
20. Peng SQ, An R, Wu ZS, Li YX (2012) Enhanced photocatalytic hydrogen evolution under visible light over $Cd_xZn_{1-x}S$ solid solution by ruthenium doping. React Kinet Mech Catal 107:105–113
21. Han C, Yang MQ, Zhang N, Xu YJ (2014) Enhancing the visible light photocatalytic performance of ternary CdS–(graphene–Pd) nanocomposites via a facile interfacial mediator and co-catalyst strategy. J Mater Chem A 2:19156–19166
22. Li Q, Li X, Wageh S, Al-Ghamdi AA, Yu J (2015) CdS/graphene nanocomposite photocatalysts. Adv Energy Mater 5:1500010
23. Wang W, Zhu W, Xu H (2008) Monodisperse, mesoporous $Zn_xCd_{1-x}S$ nanoparticles as stable visible-light-driven photocatalysts. J Phys Chem C 112:16754–16758
24. Peng XG, Manna L, Yang WD, Wickham J, Scher E, Kadavanich A, Alivisatos AP (2000) Shape control of CdSe nanocrystals. Nature 404:59–61
25. Xiao MW, Wang LS, Wu YD, Huang XJ, Dang Z (2008) Preparation and characterization of CdS nanoparticles decorated into titanate nanotubes and their photocatalytic properties. Nanotechnology 19:015706
26. Liu N, Schneider C, Freitag D, Hartmann M, Venkatesan U, Müller J, Spiecker E, Schmuki P (2014) Black TiO_2 nanotubes: cocatalyst-free open-circuit hydrogen generation. Nano Lett 14:3309–3313
27. Chowdhury P, Malekshoar G, Ray MB, Zhu J, Ray AK (2013) Sacrificial hydrogen generation from formaldehyde with Pt/TiO_2 photocatalyst in solar radiation. Ind Eng Chem Res 52:5023–5029
28. Han JF, Jian Y, He Y, Liu YN, Xiong XL, Cha LM, Krishnakumar V, Schimper HJ (2016) Nanostructures of CdS thin films prepared by various technologies for thin film solar cells. Mater Lett 177:5–8
29. Huang L, Wei ZL, Zhang FM, Wu XS (2015) Electronic and optical properties of CdS films deposited by evaporation. J Alloys Compd 648:591–594
30. Feldmeier EM, Fuchs A, Schaffner J, Schimper HJ, Klein A, Jaegermann W (2011) Comparison between the structural, morphological and optical properties of CdS layers prepared by close space sublimation and RF magnetron sputtering for CdTe solar cells. Thin Solid Films 519:7596–7599
31. Lu C, Zhang L, Zhang Y (2014) Fabrication of CdS/CdSe bilayer thin films by chemical bath deposition and electrodeposition, and their photoelectrochemical properties. Appl Surf Sci 319:278–284

32. Han J, Liao C, Cha L, Jiang T, Xie H, Zhao K, Besland MP (2014) TEM and XPS studies on CdS/CIGS interfaces. J Phys Chem Solids 75:1279–1283
33. Kariper A, Güneri E, Göde F (2011) The structural, electrical and optical properties of CdS thin films as a function of pH. Mater Chem Phys 129:183–188
34. Mukherjee A, Satpati B, Bhattacharyya SR (2015) Synthesis of nanocrystalline CdS thin film by SILAR and their characterization. Phys E Low-Dimens Syst Nanostruct 65:51–55
35. Wang J, Liu SR, Mu YN, Liu L, Runa A, Su PY, Yang JD, Zhu GJ, Fu WY, Yang HB (2017) Synthesis of uniform cadmium sulphide thin film by the homogeneous precipitation method on cadmium telluride nanorods and its application in three-dimensional heterojunction flexible solar cells. J Colloid Interface Sci 505:59–66
36. Park K, Yu HJ, Chung WK, Kim BJ, Kim SH (2009) Effect of heat-treatment on CdS and CdS/ZnS nanoparticles. J Mater Sci 44:4315–4320
37. Kim H, Kim D (2001) Influence of CdS heat treatment on the microstructure of CdS and the performance of CdS/CdTe solar cells. Sol Energy Mater Sol C 67:297–304
38. Wang J, Zhou XM, Lv P, Yang LH, Ding D, Niu JS, Liu L, Li X, Fu WY, Yang HB (2016) Influences of the CdS nanoparticles grown strategies on CdTe nanorods array films: a comparison between successive ionic layer absorption and reaction and chemical bath deposition. Electrochim Acta 202:32–36
39. Metin H, Esen R (2003) Annealing effects on optical and crystallographic properties of CBD grown CdS films. Semicond Sci Technol 18:647–654
40. Han JF, Liao C, Jiang T, Fu GH, Krishnakumar V, Spanheimer C, Haindl G, Zhao K, Klein A, Jaegermann W (2011) Annealing effects on the chemical deposited CdS films and the electrical properties of CdS/CdTe solar cells. Mater Res Bull 46:194–198
41. Vigil O, Zelaya-Angel O, Rodriguez Y (2000) Changes of the structural and optical properties of cubic CdS films on annealing in H_2 and air atmospheres. Semicond Sci Technol 15:259–262
42. Kong LJ, Li JM, Chen GL, Zhu CF, Liu WF (2013) A comparative study of thermal annealing effects under various atmospheres on nano-structured CdS thin films prepared by CBD. J Alloys Compd 573:112–117
43. Flores-Marquez JM, Albor-Aguilera ML, Matsumoto-Kuwabara Y, Gonzalez-Trujillo MA, Hernandez-Vasquez C, Mendoza-Perez R, Contreras-Puente GS, Tufiño-Velazquez M (2015) Improving CdS/CdTe thin film solar cell efficiency by optimizing the physical properties of CdS with the application of thermal and chemical treatments. Thin Solid Films 582:124–127
44. Maticiuc N, Spalatu N, Mikli V, Hiie J (2015) Impact of CdS annealing atmosphere on the performance of CdS–CdTe solar cell. Appl Surf Sci 350:14–18
45. Goto F, Shirai K, Ichimura M (1998) Defect reduction in electrochemically deposited CdS thin films by annealing in O_2. Sol Energy Mater Sol C 50:147–153
46. Yu Z, Yin BS, Qu FY, Wu X (2014) Synthesis of self-assembled CdS nanospheres and their photocatalytic activities by photodegradation of organic dye molecules. Chem Eng J 258:203–209
47. Li XY, Hu CG, Wang X, Xi Y (2012) Photocatalytic activity of CdS nanoparticles synthesized by a facile composite molten salt method. Appl Surf Sci 258:4370–4376
48. Bhadwal AS, Tripathi RM, Gupta RK, Kumar N, Singh RP, Shrivastav A (2014) Biogenic synthesis and photocatalytic activity of CdS nanoparticles. RSC Adv 4:9484–9490
49. Xie YB (2006) Photoelectrochemical reactivity of a hybrid electrode composed of polyoxophosphotungstate encapsulated in titania nanotubes. Adv Funct Mater 16:1823–1831
50. Li HY, Sun YJ, Cai B, Gan SY, Han DX, Niu L, Wu TS (2014) Hierarchically Z-scheme photocatalyst of Ag@AgCl decorated on $BiVO_4$ (0 4 0) with enhancing photoelectrochemical and photocatalytic performance. Appl Catal B Environ 170–171:206–214
51. Huang HW, Li XW, Han X, Tian N, Zhang YH, Zhang TR (2015) Moderate band-gap-broadening induced high separation of electron–hole pairs in Br substituted BiOI: a combined experimental and theoretical investigation. Phys Chem Chem Phys 17:3673–3679
52. Wang YB, Wang YS, Xu R (2013) Photochemical deposition of Pt on CdS for H_2 evolution from water: markedly enhanced activity by controlling Pt reduction environment. J Phys Chem C 117:783–790